AN ASSESSMENT OF THE DISTRIBUTION OF LANDSLIDES CAUSED BY DEBRIS FLOWS IN FAIFA MOUNTIANS, JAZAN AREA, SAUDI ARABIA USING REMOTE SENSING AND GIS TECHNIQUES

Prepared by

Talal Alharbi

Graduate Student

Advisor

Dr. Mohamed Sultan

Department of Geosciences

Western Michigan University

1. Introduction

The Arabian Peninsula consists of two groups of rocks, the Arabian Shield and the Arabian Shelf (Fig 1a). The Arabian Shield is located in the western side of the Peninsula. It is mainly formed of Precambrian complex of igneous and metamorphic rocks that is cover one-third of the Arabian Peninsula. This group of rocks is uncomfortably overlain by the Arabian Shelf that is Paleozoic, Mesozoic, and lower Tertiary sedimentary successions. These sedimentary formations are exposed in central Arabia in a great curved belt bordering the Arabian Shield and dip gently and uniformly away from the Shield towards the Arabian Gulf in the east and Rub Alkhali basin in the southeast. (Powers et al., 1966).

The southwestern parts of the Kingdom are quite different from the remaining arid to semi arid parts of the Kingdom as they receive high amounts of precipitation (up to 700 mm/year). The study area, the Jizan, lies within the southwestern part of the Kingdom. Jizan Region (latitude: 16.5-17.7°N; Longitude: 42.0-43.8° E) is located in the southern parts of the Arabian shield (500 to 900 MA) on the borders of the Kingdom with Yemen (Fig. 1a). The Jizan area (13,500 km^2) is characterized by three distinct topographic zones (Alehaideb, 1985). These include, the Red Sea coastal plain (Tihama) to the west, the Hijaz plateau to the east, and the Hijaz Mountains in between the coastal plain and the plateau (Fig. 1b). The Tihama coastal area is a relatively flat and wide (40 km) terrain that is characterized by hot and humid climate. The Hijaz mountains are high (1600 to 3000 m a.m.s.l) and extensive (width: 140 km) characterized by temperate climates. The Hijaz plateau is mainly flat area with moderate elevations (200 to 1800 m a.m.s.l) and progressively warmer temperatures inland. The rock in the Hijaz Mountains

are largely composed of granite, diorite, gabbro, basalt, syenite and micaschist that are all parts of the basement complex, whereas the Tihama coastal area is largely composed of alluvial deposits (muddy sand, sandy mud, silt, clayey silt and silty clay)(Abou Ouf, 1992).

The study area, Faifa Mountains located in the southern region of Jazan in the Hijaz Mountains. These mountains are the highest peaks in the area, which rises 1810 m above sea level. Faifa Mountains have harsh land nature. In many parts of these mountains there are steep slopes (up to 71°) and receive more than 800 mm of precipitation/yr (Fig. 2c). After a heavy rainfall event, surface runoff mobilizes detritus from the mountains and transports the load within ephemeral valleys that drains the surface water down the mountains.

The discovery of oil in the Kingdom of Saudi Arabian signaled an important era in the construction of new urban centers and networks of highways to connect the newly developed urban centers and the scattered remote villages across the entire length of the Kingdom. Faifa Mountains in Jazan like the rest of the Arabian Shield cities witnessed construction of highways, roadcuts, and bridges to connect these remote mountainous terrains to the coastal plain. The high precipitation in these areas, and the intensified construction phase lead to landslide development in the Faifa mountains. In this paper, I examine the distribution and nature of landslides, and the factors controlling their development. Also, I construct landslide hazard distribution maps for Faifa Mountains.

2. Landslides Types and methodologies to detect them

This study is largely based on observations extracted from remotely acquired data sets and products and limited field data. My approach depends on: (1) Examination of known landslide locations in the field and/or from high resolution remote sensing data sets and characterization of their type, (2) extraction of criteria to enable identification of the known landslide locations using remote sensing data sets, (3) using the selected criteria I identified areas where similar landslide types could occur elsewhere in the study area. The latter activity entails the construction of a hazard map that shows the relative likelihood for the occurrence of each of the identified landslide types across the investigated area. On these maps, the likelihood for the occurrence of a landslide is dictated by the intensity of one or more of the factors controlling their occurrence. Examples of these factors include slope amount and direction, fracture plane dip and direction, vegetation intensity, and man-made structures (Cruden, 1996). Our field verification program was conducted over two field trips, hereafter referred to as field trip I and field trip II. Field trip I was conducted on January, 2011 and field trip II on January, 2012. During this trip I was shown a number of selected locations for known landslides in the area. Figure 2a shows the distribution of landslide locations that were visited during field trip I (landslide #1, 2, and 23) and a selected suite of similar landslide types that were identified (landslide #1-7, 11, 13, 14, 16, 18, 20, 22, 23) using procedures described above. In field trip II, I visited all of the landslides locations that were identified and selected from remotely acquired data (Figure 2b).

To conduct steps 1 through 3, I had to produce many derived image products that display important topographic and spectral characteristics of interest that could be used for the identification of landslide locations. Examples include: disruption of contoured

elevations, decrease in vegetation, and high spectral reflectance within areas affected by landslides. Contoured elevation maps were derived from topographic sheets provided by the SGS (Saudi Geological Survey) with 10m contour interval. Investigating the intensity of vegetation in an area was enabled by examining NDVI images which were extracted from spectral reflectance images which were in turn derived from raw DN (digital number images) of SPOT multispectral images. Additional products were generated to evaluate the hazards associated with the identified landslide types. For example, to evaluate the hazards associated with debris flow associated with ephemeral streams on the road network and existing structures, maps showing the distribution of houses, and roads were generated.

3. Landslides caused by debris flows within ephemeral valleys intersecting roads and buildings

Debris flows are often of high density, with over 80 percent solids by weight, and may exceed the density of wet concrete (Hutchinson, 1988). They can move boulders that are meters in their diameter. Debris flow occurs during torrential runoff following exceptional rainfalls. Soils on steep slopes that are unprotected by vegetation are prone to debris flows (Cruden, 1996).

Our observations from field trip I and examination of remotely acquired data sets led us to identify a number of the visited landslides as being caused by debris flows that originated by abrupt floods of water that undermined and incorporated sediments. This conclusion is supported by: (1) the localization of debris along discrete channels, (2) landslides are all in high elevations (> 800 m a.m.s.l), where the slope gradients are

quite steep (35° to 38°), and (3) precipitation over these steep mountains is high (863 mm/yr) (Fig. 2c) and will be channeled in the ephemeral valleys towards the lowlands (Cruden, 1996). Given the steep surface gradient in the study area and the high precipitation over the mountainous area one would expect a heavy sediment load to be carried to the lowlands by the ephemeral streams crosscutting these mountains. If theses streams cross any of the constructed roads without having appropriate drainage construction under the road, the carried sediment, the landslide, will destruct the road. Figure 3 is satellite image that show one of such landslides for the debris flows along ephemeral stream that intersected a road. To identify these locations a number of product maps were generated including: road and house map, ephemeral stream map, flow accumulation map. These maps were then used to extract two hazard maps, one showing the intersection of streams with roads and the other the intersection of streams with house. In this analysis I considered all intersections of streams to be hazardous to some extent.

3.1 Road and house map

The generated map shows the distribution of roads in the study area. These include

roads and the distribution of houses (Fig. 4). The houses were digitized manually from Google Earth and GeoEye image.

3. 2 Ephemeral stream map

The map shows the distribution of ephemeral streams in the study area (Fig. 5). Figure 5 was generated using standard techniques for stream delineation such as the TOPAZ technique (Garbrecht and Martz, 1997). This technique compares the elevation of each

pixel to its surrounding eight points. These comparisons will allow the identification of the direction to which the water will flow. It is from the central pixel to the surrounding pixel that has the lowest elevation of the surrounding eight pixels. The process is repeated until the streams are delineated across the entire image. The accuracy of the delineated streams will depend largely on the spatial resolution of the DEM used, the finer the spatial resolution, the better and vice versa.

Flow accumulation map (Fig. 6): The map shows the flow accumulation. The flow accumulation is a term that provides a count for the number of pixels that drain towards a certain pixel. For example, an outlet of a watershed will have the largest numbers of pixels draining to it when compared to all other pixel within the investigated watershed (Chang, 2006). In Figure 6, the dark pixels are the ones with a large numbers of pixels draining to them.

Inspection of the Fig. 6 shows that as expected, the highest flow accumulations are to be found along the streams. The flow accumulation image is a bi-product that could be extracted using standard GIS techniques as one attempts to delineate stream networks automatically. One would expect that the landslides are more likely to occur in the high flow accumulation zones. This product (flow accumulation) was produced to be utilized in the generation of the hazard maps presented here.

3.3 Hazard maps for debris flows within ephemeral valleys

Runoff in the ephemeral streams could be hazardous to roads if: (1) these streams intersect the roads, and (2) drainage systems were not set in place. Likewise the runoff in the stream could be hazardous to buildings (e.g., houses) if: (1) these buildings were

constructed proximal to the stream channels, and if (2) appropriate drainage systems were not installed. In both cases, I can test for the first condition using remote sensing data, but not the second.

Thus, I produced two hazard maps (Figs. 7a and 7b) in which intersection of streams with roads and buildings.

Figure 7a is a hazard map that shows the intersection of all buffered streams with roads. I found 3455 intersections of streams with roads. These should be inspected in the field to find out whether proper drainage systems were installed in these intersections or not.

Figure 7b is a hazard map that shows the intersection of all buffered streams with houses. The buffering distance on either side of the streams was based on the order of the stream, the higher the stream order, the larger the buffer zone. For example, streams that have an order of one were assigned a one meter buffer distance on either side of the stream, and the second order streams were assigned a two meter buffer distance. Stream orders in the study area ranged from 1 to 7. I mapped a total of 7984 houses, of which 430 houses were found to be within the buffered stream zones. Again, these should be inspected in the field to examine whether proper drainage systems were in place or not and to examine whether the assigned buffer zone was appropriate. For example, the assigned buffer zone (based on streams order) might not be appropriate in all areas. The assumption I make is that the flow accumulation correlates with the stream order, the higher the order, the greater the stream accumulation and vice versa. Although true in most cases, there are exceptions to this rule.

Naturally, a number of these will turn out to be false alarms. For example, I found in field trip II that a number of the identified house locations at intersections with streams were on higher grounds than the streams that presumably intersect them. These types of false alarms were more pronounced for houses on high ground elevations. Unfortunately, these observations can not be easily extracted from available remote sensing data. Initially, I used a single buffer distance (5m) regardless of the order of the stream. Upon inspection in the field, I realized problems with such assignment, there were a number of false alarms. Many of these were omitted once I started using the order-dependant buffer distance. I used a buffer of 1 meter for the first order, two meters for the second order and so on. These were based on field and satellite-based observations. It is important that field inspections should be conducted to verify the validity of each of the intersections. It is noteworthy to mention that despite the difficulties stated above, our field inspections in field trip II showed that all space-borne stream/road intersections are valid and approximately 60% of the stream/house intersections are true. Since then, I refined our methodology by using a DEM with higher spatial resolution (10m as opposed to 30m) which enabled us to better delineate the stream networks and to calculate more realistic flow accumulation values.

Not all of the identified streams will be sites for debris flows. One would expect that in general, the steeper the slope along the identified streams, the more likely the debris flow will occur. Another condition that I set for the debris flow to occur is sparse vegetation. The lesser the vegetation, the more likely that the stream will be effective in transporting debris down slope (Horton, 1933; Scott 1971; Wells et al. 1987; Weirich 1989; Florsheim et al. 1991). Only barren or nearly barren slopes along the identified

stream were considered as subject to debris flows. The third condition has to do with the presence or absence of terraces. Debris flows are less likely to occur in areas where terraces were established. Terraces have the effect of increasing infiltration and reducing runoff. Three additional digital products were generated: NDVI, slope, and terrace distribution and were used to generate a hazard map that reflects the probabilities for debris flow along overland flows. Debris flow could be identified visually verified from Google Earth images.

3.4 Slope distribution and histograms

Figure 8a shows the distribution of streams and slopes. The slope image was created from a 10m digital elevation model. The distribution of slopes could be represented by standard statistical methods (mean and standard deviation). Figure 8b shows that the mean slope in the area is 23° and the standard deviation is 13°. The steepest slopes are to be found on the mountain sides surrounding the valleys. Areas over these mountain sides that have steep slopes are prone to mass movement (i.e., landslides) initiated by debris flow.

3.5 NDVI distribution and histogram

There are additional factors that could contribute to mass movement on these steep slopes. One of these factors is the paucity of vegetation. The absence or paucity of vegetation can facilitate the movement of detritus with overland flows (Glancy and Harmsen 1975). The construction of buildings in these areas could be hazardous. I generated Normalized Difference Vegetation Index (NDVI) images from SPOT data (spatial resolution: 2.5 m) that provide a measure for the intensity of vegetation, the

higher the NDVI values for a picture element, the more extensive the vegetation and vice versa (Rouse, 1973). The NDVI values for the study area range from -0.17 to +1.0. It is known that areas with NDVI values of -0.1 to 0.09 are usually considered as barren rocks or dry soils (Jackson, 1991). During field trip II, I visited areas with NDVI values of 0.09 or less and found that all of these areas were barren or have very sparse vegetation.

The NDVI image is constructed as follows:

NDVI = (NIR — VIS)/(NIR + VIS)

Where:

NIR refers to reflectance in a near infrared band (SPOT band 3)

VIS refers to reflectance in a visible band (SPOT band 2).

Figure 9a shows NDVI image for the study area. Areas of high NDVI (shades of green) are less prone to debris flow, whereas areas of low NDVI values (shades of brown) are more prone to debris flow. Figure 9b is a histogram for NDVI distribution in the study area.

3.6 Distribution of terraces

In some of these steep slope areas, the locals modify the slopes by building more stable structures called terraces. These structures enhance infiltration and reduce runoff (Naderman, 1990). Based on our field observations and analysis of Google Earth images, I reached the conclusion that areas covered by terraces are stable areas that

are not prone to debris flow. Figure 10 shows the distribution of terraces in the study area.

3.7 Hazard map showing distribution of areas prone to debris flow:

As described above the larger the slope and the lesser the vegetation, the greater the chances for debris flows to occur. I extracted a relationship for the study area that adequately describes the interplay between these two factors, the intensity of vegetation and the steepness of the slope. Using known locations of debris flows (from field and satellite observations), I extracted the slopes and NDVI values for picture elements (pixels) that I identified as representing the onset points for each of these debris flows. These values were plotted on an X-Y plot, where the slope is plotted on the X-axis and the NDVI value on the Y axis. The extracted slope ranged from 29° to 42° and averaged 35°, whereas the NDVI values ranges from -0.04 to 0.24 and averaged 0.07. A linear regression was then used to identify the equation of a straight line that best fitted the points with the steepest slope and the smallest NDVI values (Fig. 11). Knowing the equation of the straight line, I can then substitute all pixels of all streams in the equation to test whether the examined stream pixel is on the line (value = 0), above the line (value: +ve), or below the line (value: -ve). A coverage was constructed from points that are on or above the line; this coverage represent locations along mapped stream lines that are susceptible to debris flow. An additional condition was enforced, the positive points had to be outside the areas mapped as terraces. Points falling below the line were considered to be susceptible to debris flow. Figure 12 shows the distribution of areas prone to debris flows.

4. Findings and Conclusions

I adopted an integrated (field, GIS, and remote sensing) approach to map the distribution of landslides and to identify their controlling factors in Faifa Mountains in the Jazan area, Red Sea Hills, Saudi Arabia. Our approach depends on: (1) Identification and characterization of known landslide locations using field and/or high resolution remote sensing data sets, (2) extraction of criteria to enable identification of the known landslide locations using remote sensing data sets, (3) using the selected criteria to identify areas where similar landslide types could occur elsewhere in the study area. To conduct steps 1 through 3, I produced several derived image products that were used to identify areas that are prone to, or witnessed mass movement. For example, areas prone to movements have low vegetation (NDVI image) and steep slopes (slope image). Areas that witnessed mass movement are less vegetated than their surroundings and hence are bright compared to their vegetated dark surroundings on reflectance images and show evidence of disruption on contour maps. Investigating the intensity of vegetation in an area was enabled by examining NDVI images which were extracted from spectral reflectance images of SPOT multispectral images. Contoured elevation maps (contour interval: 10 m) were derived from available landuse maps. Additional products were generated to evaluate the hazards associated with the road network and houses. The study identified the main type of landslides in the study area, landslides caused by debris flows within ephemeral valleys that could be hazardous to the roads and buildings they intersect. I found 3455 intersections of streams with roads and 430 houses were found to be within the stream zones. I developed criteria that allowed the the identification of the ephemeral valleys that are likely to develop debris

flows and used these criteria to generate hazard maps across the study area for areas prone to mass movement (debris flow). Implications for the utilization of this integrated approach in similar settings elsewhere are clear.

5. Acknowledgements

My great appreciation to Dr. Mohamed Sultan for supervising this research and for assisting in the field work.

References

Abou Ouf MA, El Shater A (1992) Sedimentology and mineralogy of Jizan shelf sediments, Red Sea, Saudi Arabia. JKAU: Mar Sci 3:39–54.

Alehaideb, I. (1985) Rainfall distribution in the southwest of Saudi Arabia. PhD Thesis, Arizona State Univ., Arizona, USA.

Barton, N.R. 1973. Review of a new shear strength criterion for rock joints. Eng. Geol. 7, 287-332.

Barton, N.R. 1974. A review of the shear strength of filled discontinuities in rock.

Norwegian Geotech. Inst. Publ. No. 105. Oslo: Norwegian Geotech. Inst.

Casals, J.F., 1986, Analysis of a landslide along Interstate 70 near Vail, Colorado: Golden, Colorado School of Mines, Master's thesis, 121 p.

Chang, K-t, 2006, Introduction to geographic information system, 3rd edition McGraw Hill, 432 pp.

Cruden, DM & Varnes, DJ. 1996. Landslide types and processes. In Special Report 247: Landslides: Investigation and Mitigation, Transportation Research Board, Washington D.C.

Florsheim, J. L., E. A. Keller, and D. W. Best (1991), Fluvial sediment transport in response to moderate storm flows following chaparral wildfire, Ventura County, southern California, Geol. Soc. Am. Bull., 103(4), 504 – 511.

Garbrecht, J. and L.W. Martz, 1997. TOPAZ Version 1.20: An automated digital landscape analysis tool for topographic evaluation, drainage identification, watershed segmentation and subcatchment parameterization - Overview. Rep.# GRL 97-2, Grazinglands Research Laboratory, USDA, Agricultural Research Service, El Reno, Oklahoma, 21 pp.

Glancy,P.A., and Harmsen,L., 1975, A hydrologic assessment of the September 14, 1974 flood in Eldorado Canyon, Nevada: U.S. Geological Survey Professional Paper 930, 23p

Horton RE. 1933. The role of infiltration in the hydrologic cycle. Transactions, American Geophysical Union 14: 446–460.

Hutchinson, J. N. 1988. General Report: Morphological and geotechnical parameters of landslides in relation to geology and hydrogeology. Proceedings, Fifth International Symposium on Landslides (Ed: Bonnard, C.), 1, 3-35. Rotterdam: Balkema.

Jackson, R.D. and Huete, A.R., 1991. Interpreting vegetation indices. Prev. Vet. Med., ll: 185-200.

Jaeger, J. C. and N. G. W. Cook, Fundamentals of Rock Mechanics, 2nd ed.,593 pp., Chapman and Hall, London, 1976.

Keaton JR and DeGraff JV (1996) Surface observation and geologic mapping. In: Turner AK and Schuster RL (eds), Landslides, Investigation and Mitigation. Washington, DC, Transportation Research Board Special Report 247, pp. 178-230.

Lowell, Steve M., 1990, The K M Mountain landslide near Skamokawa: Washington Geologic Newsletter, v. 18, no. 4, p. 3-7.

Naderman, G.C., J.R. Hansard, and H.P. Denton. (1990). Surface water management for crop production on highly erodible land. Applied Agricultural Research, 5 (4).

Norrish. N.I. and Wyllie. D.C. (1996). Rock slope stability analysis. In Landslides: Investigation and Mitigation – Special Report 247. National Academy Press: Washington, D.C., pp. 391-425.

Powers R. W., Ramirez L. F., Redmond C. D. and Elberg E. L. 1966. Geology of the Arabian Peninsula, Geological Survey Professional Paper, 560-D: 1-147.

Rouse, J.W., Jr., R.H. Haas, J.A. Schell, and D.W. Deering. 1973. Monitoring the vernal advancement and retrogradation (green wave effect) of natural vegetation. Prog. Rep. RSC 1978-1, Remote Sensing

Scott, K. M. (1971). Origin and Sedimentology of 1969 debris flows near Glendora, California. Geol. Surv. Prof. Pap. (U.S.) 750-C, C242-C247.

Weirich, F.H. 1989: The generation of turbidity currents by subaerial debris flows, California . Geological Society of America Bulletin 101, 278–291

Wells, W.G., II, Wohlgemuth, P.M., Campbell, A.G., and Weirich, F.H., 1987, Postfi re sediment movement by debris fl ows in the Santa Ynez Mountains, California, in Erosion and sedimentation in the Pacifi c Rim: Proceedings of the Corvallis Symposium, International Association of Hydrologic Sciences Publication no. 165, p. 275–276

Wylie, D.C.,(1992). Foundations on Rock. 1st ed., Chapman and Hall, London, 331 pp.

Wyllie, D.C. & Norrish, N.I. (1996). Rock strength properties and their measurement. In Landslides: Investigation and Mitigation – Special Report 247. National Academy Press: Washington, D.C., pp. 372-3790.

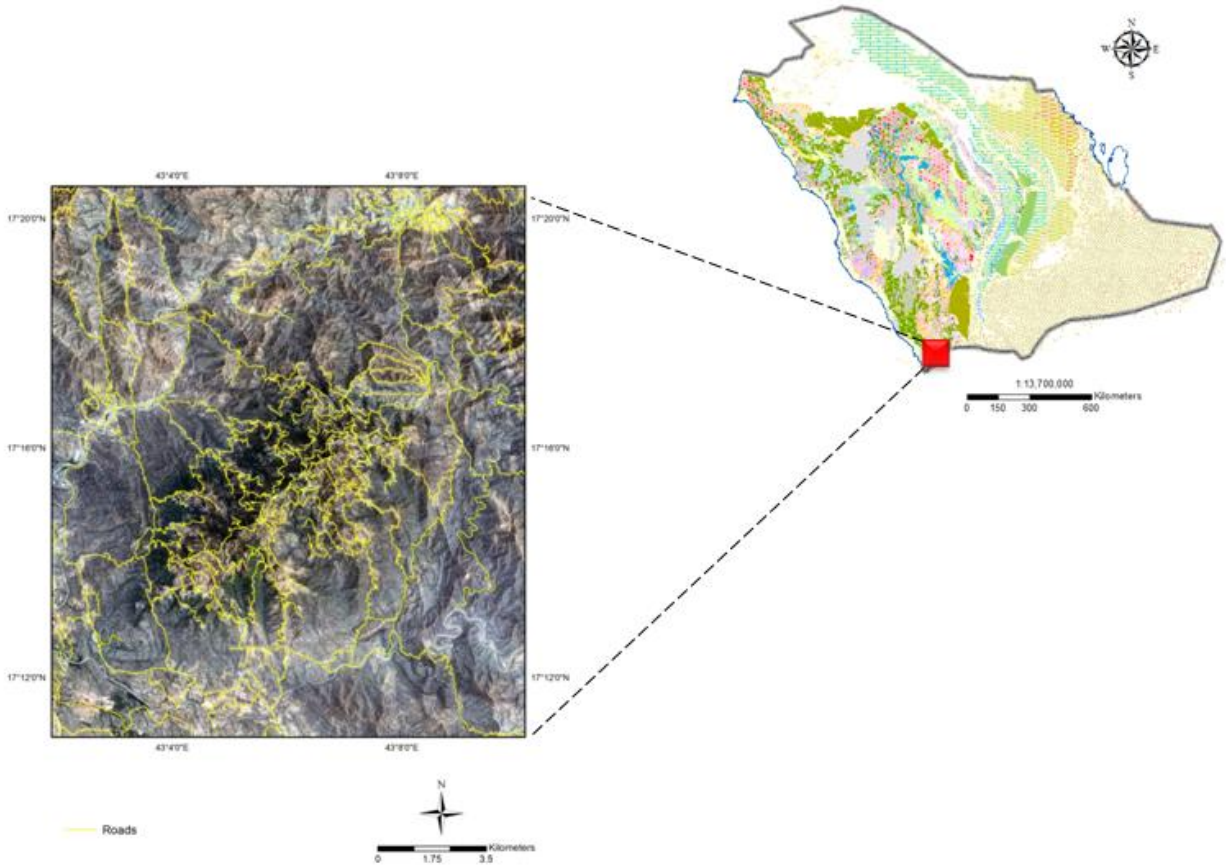

Figure 1a. Location map of the study area.

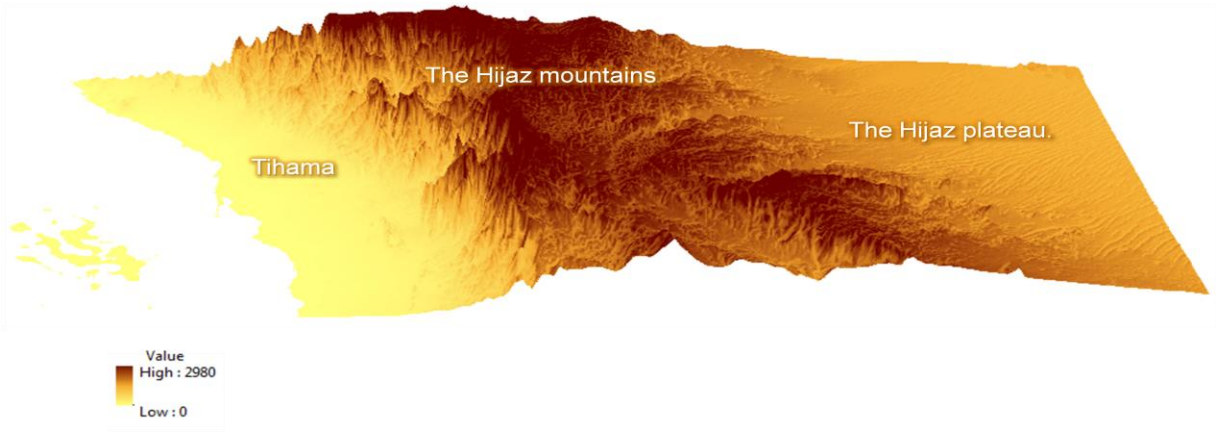

Figure 1b. Location map of the three zones in Jizan area.

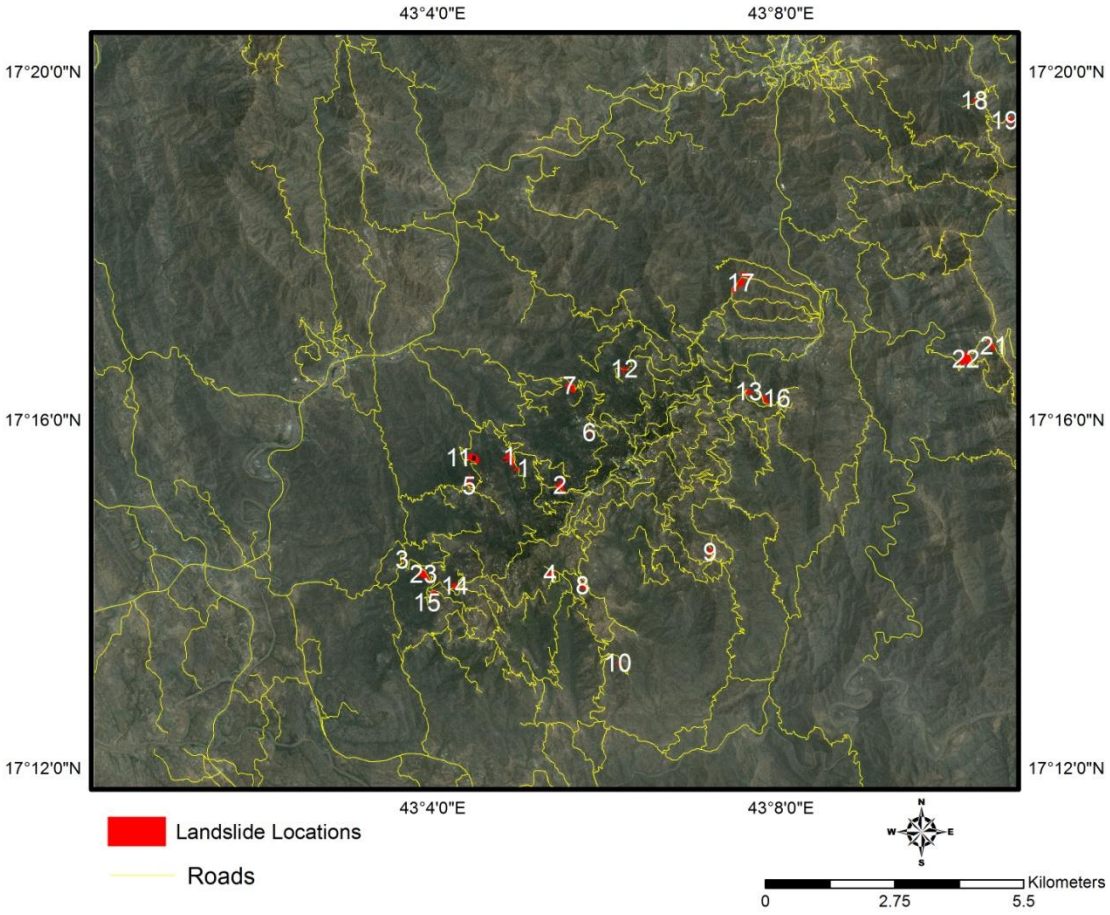

Fig. 2a. Locations of landslides that were visited in the field and a selected suite of similar landslides that were extracted from remotely acquired data.

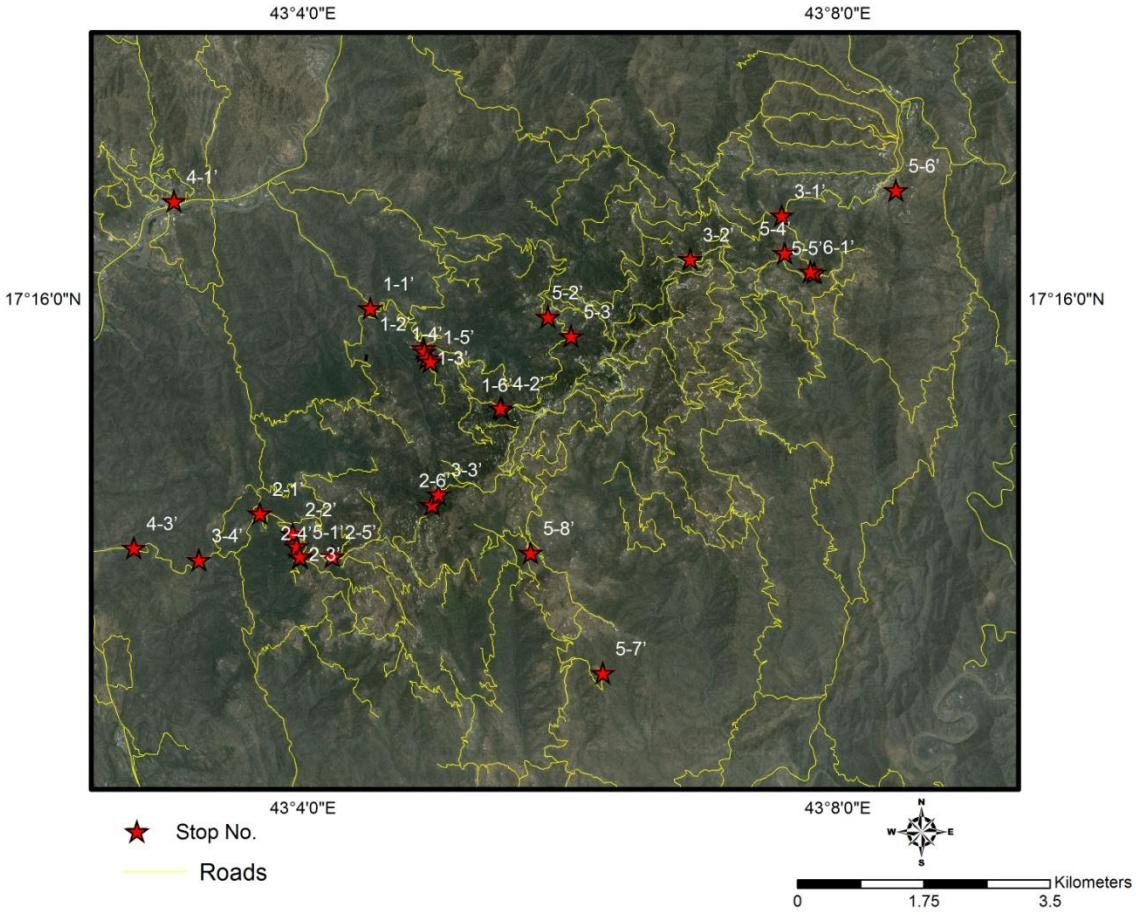

Fig. 2b. Locations of stops that were visited in field trip II.

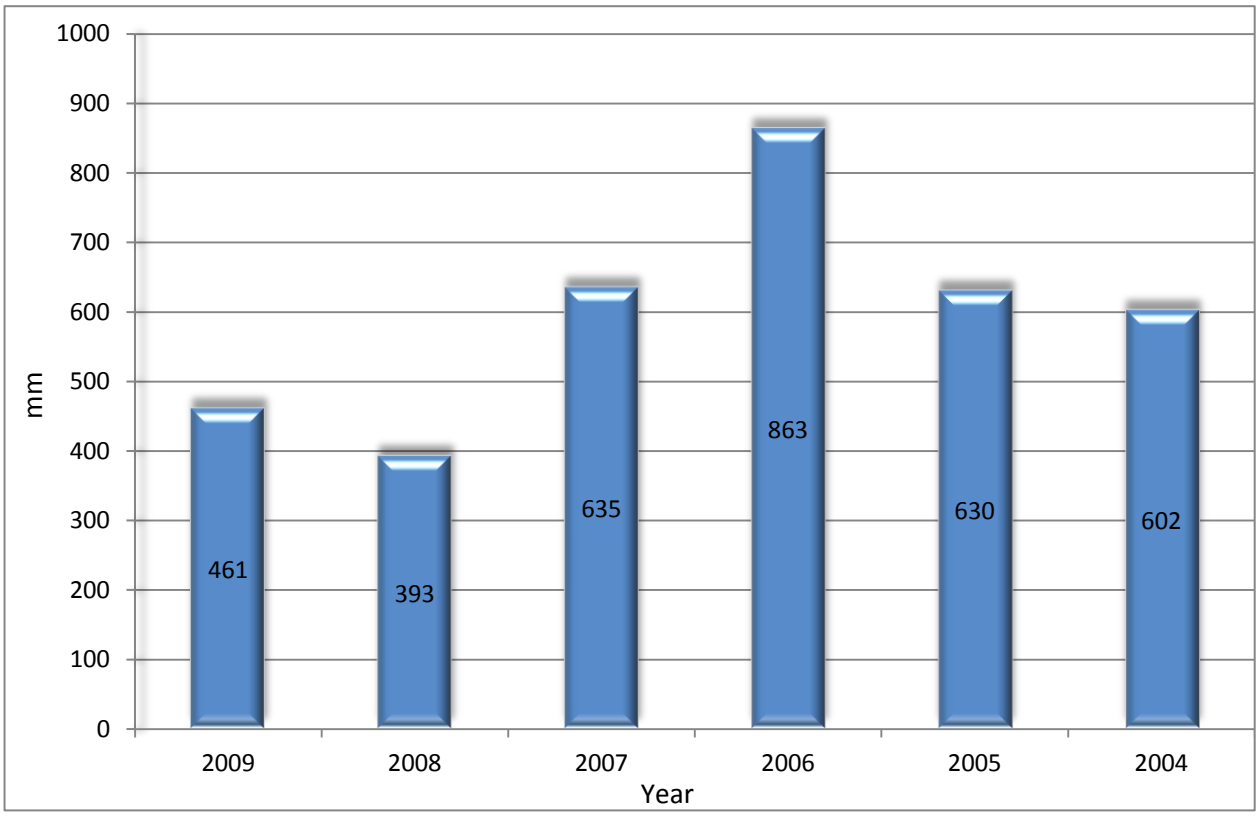

Figure 2c. Faifa average annual precipitation.

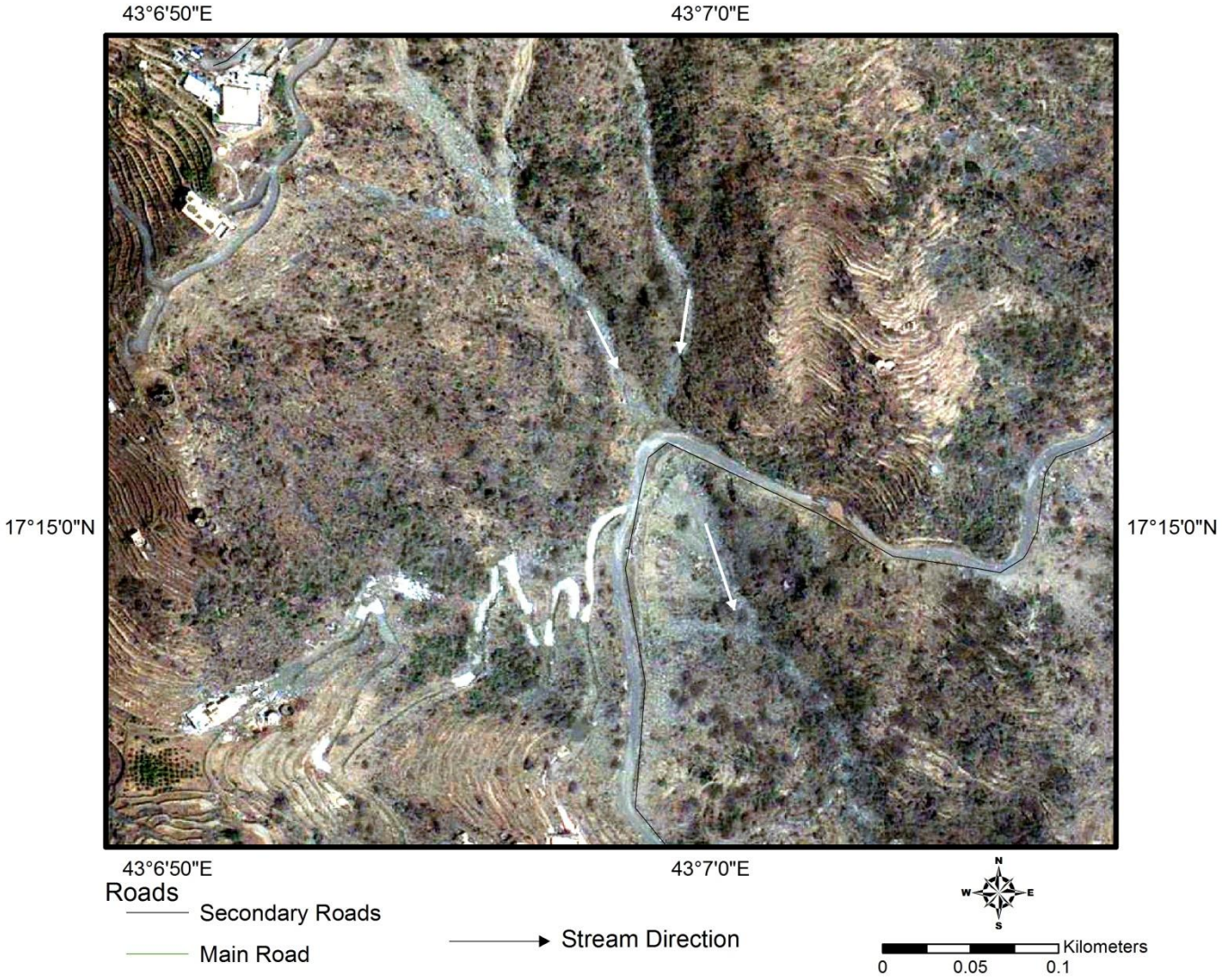

Figure 3. A satellite image showing ephemeral stream that intersect a road.

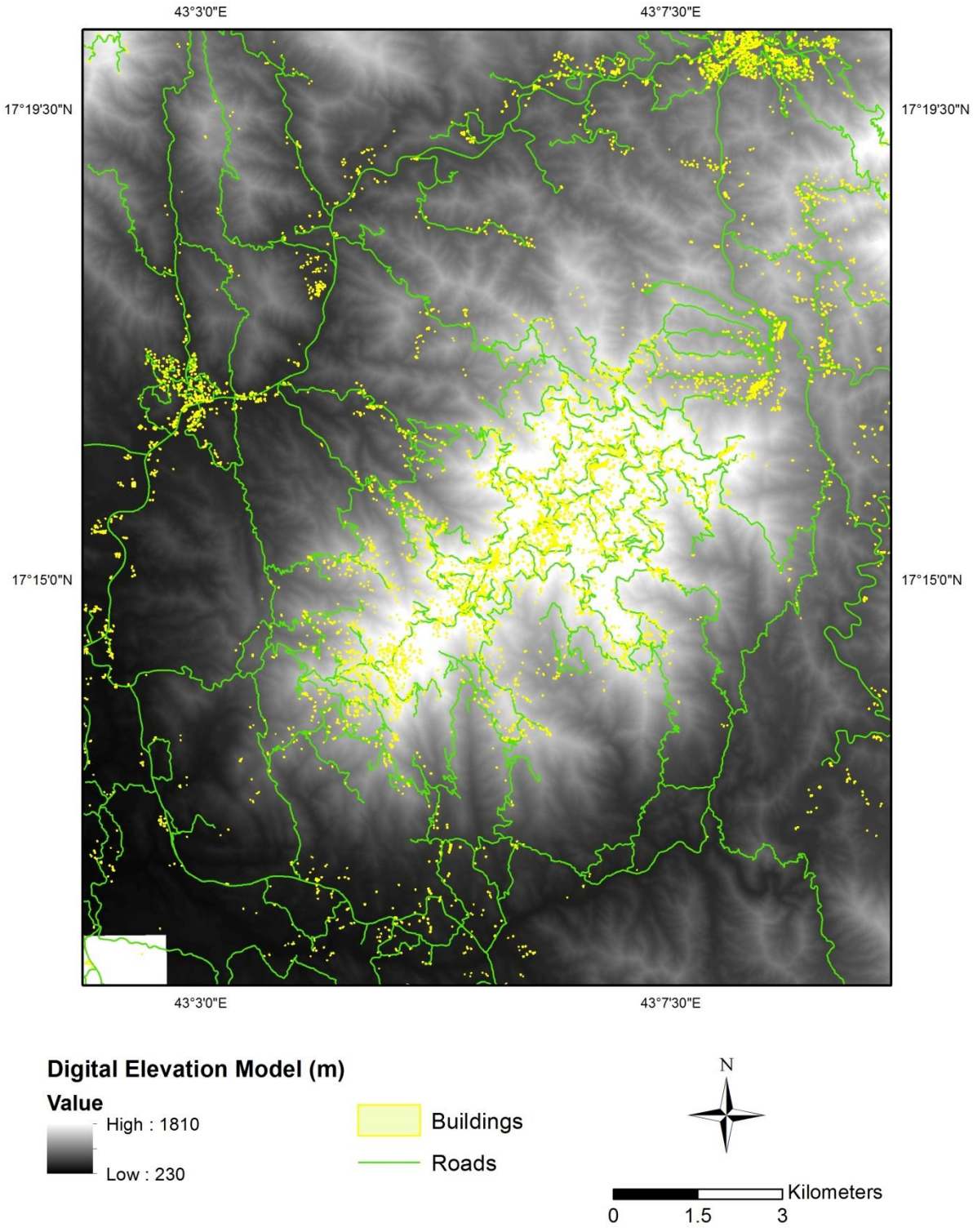

Figure 4. Distribution of roads and buildings extracted manually from Google Earth maps.

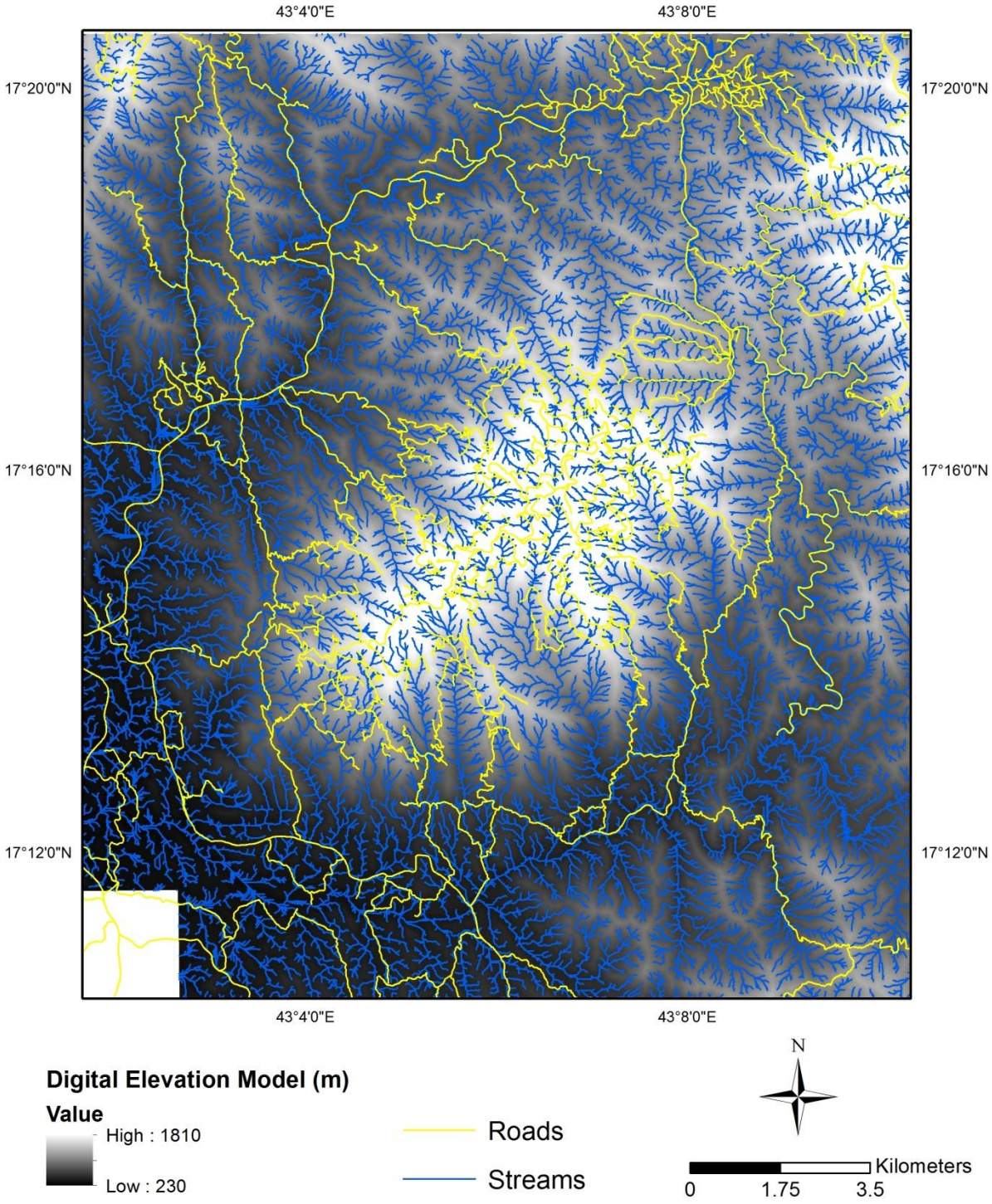

Figure 5. Stream distribution extracted from 10m DEM overlain onto black and white coded digital elevation image.

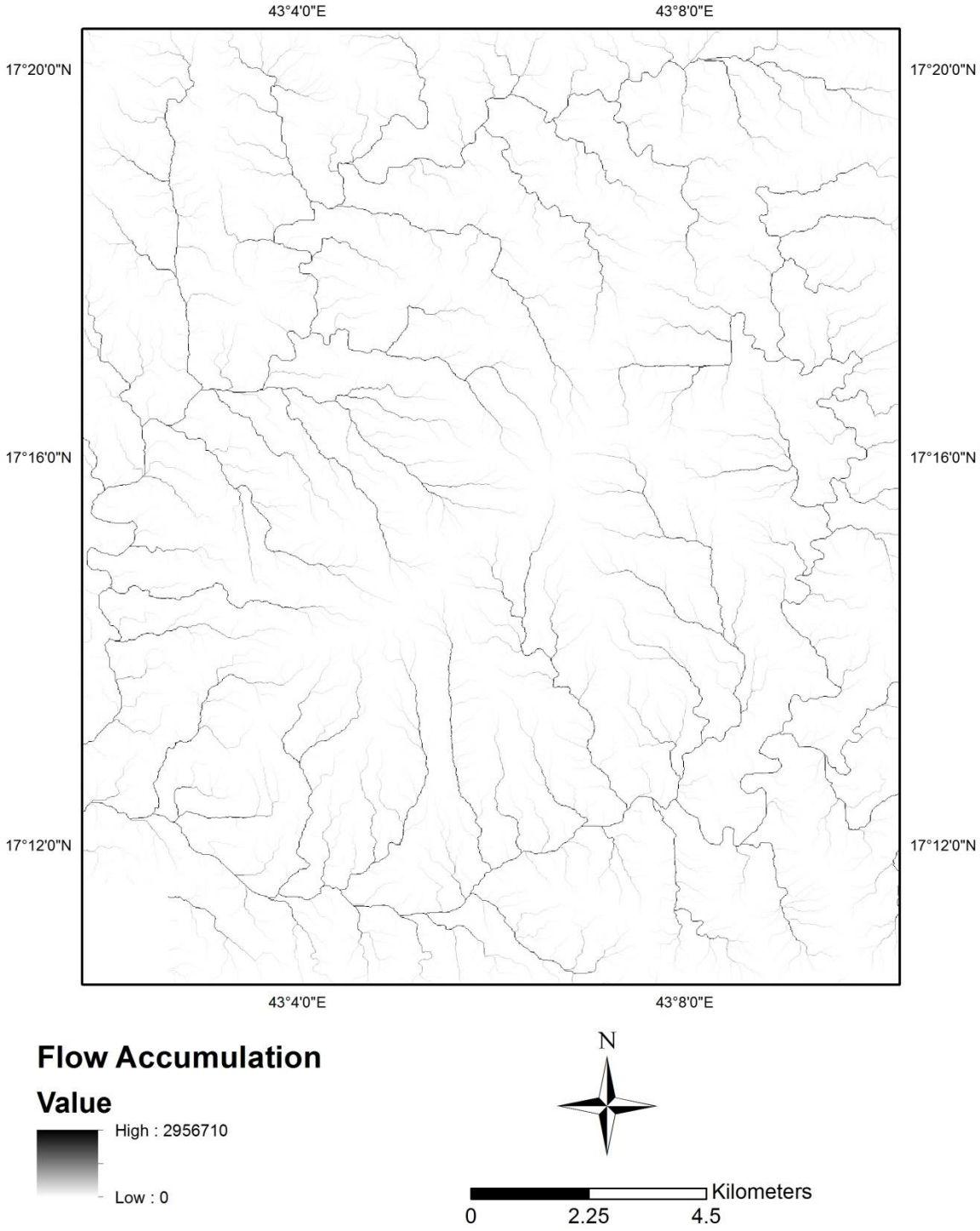

Figure 6. Flow accumulations extracted as a bi-product in the process of delineating the streams using standard GIS techniques. The flow accumulation is reported in number of cells where one cell has a size of 10X10 m.

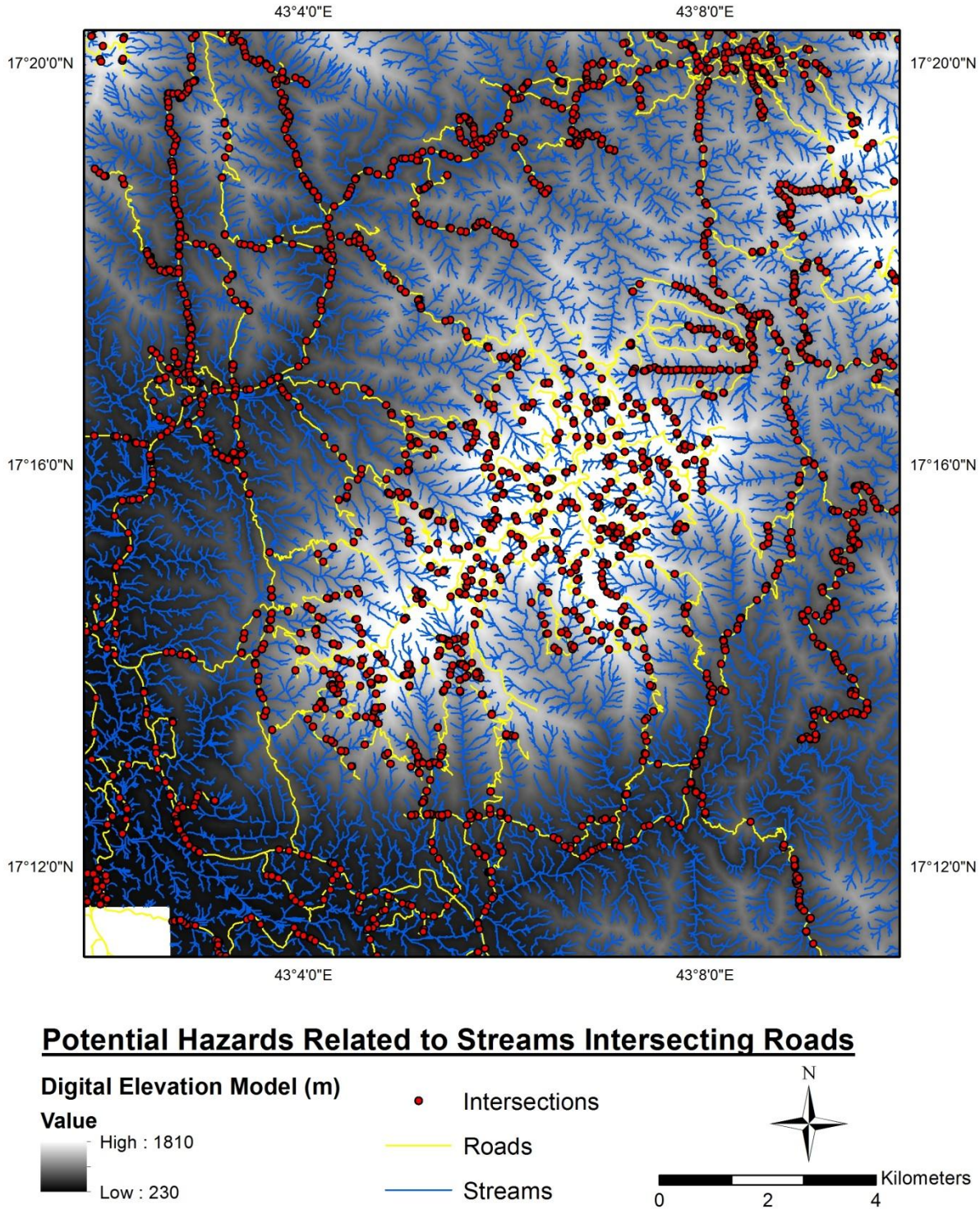

Figure 7a. Hazard map showing the intersections buffered streams with roads.

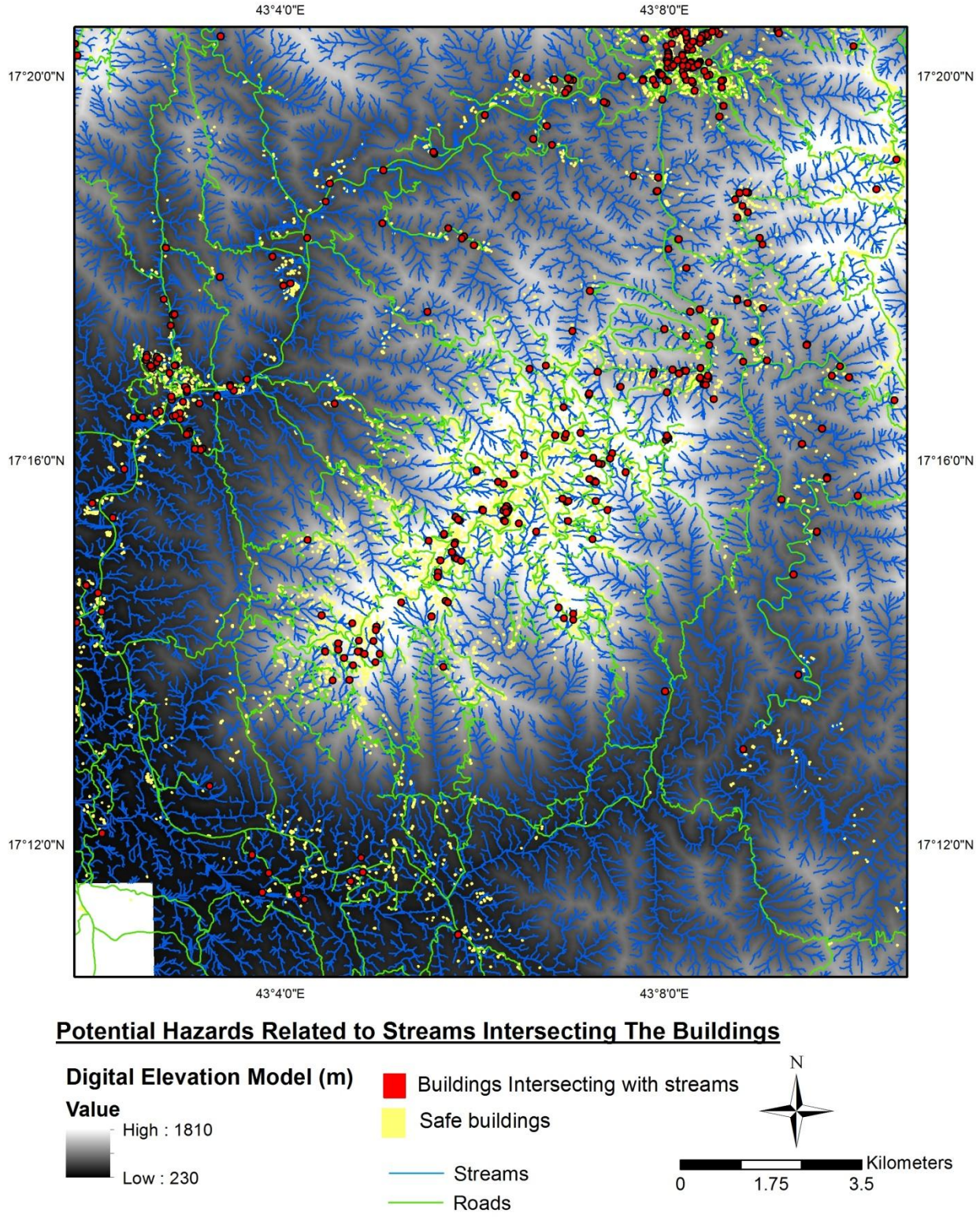

Figure 7b. Hazard map showing the intersections of buffered streams with buildings.

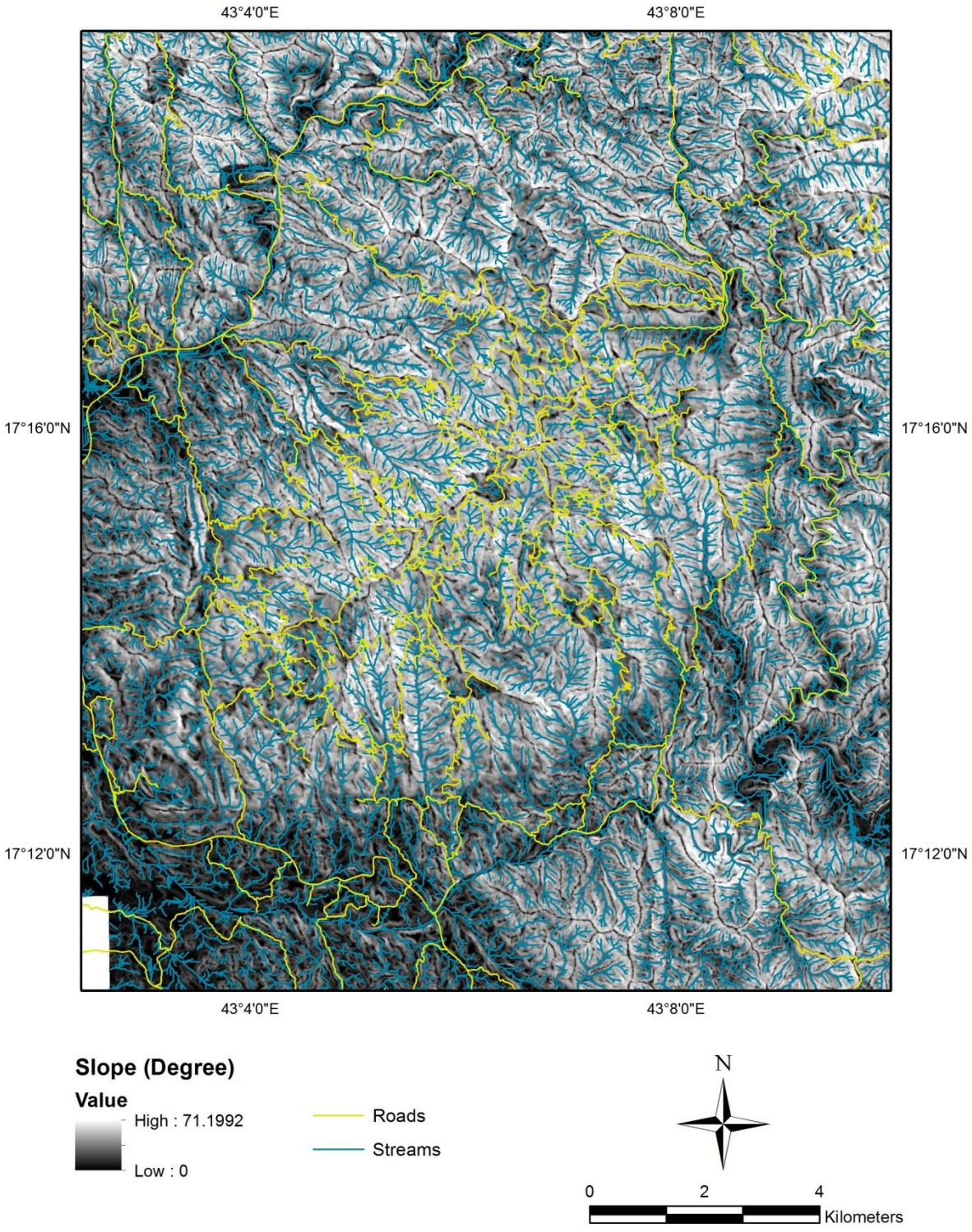

Figure 8a. Distribution of streams and slopes

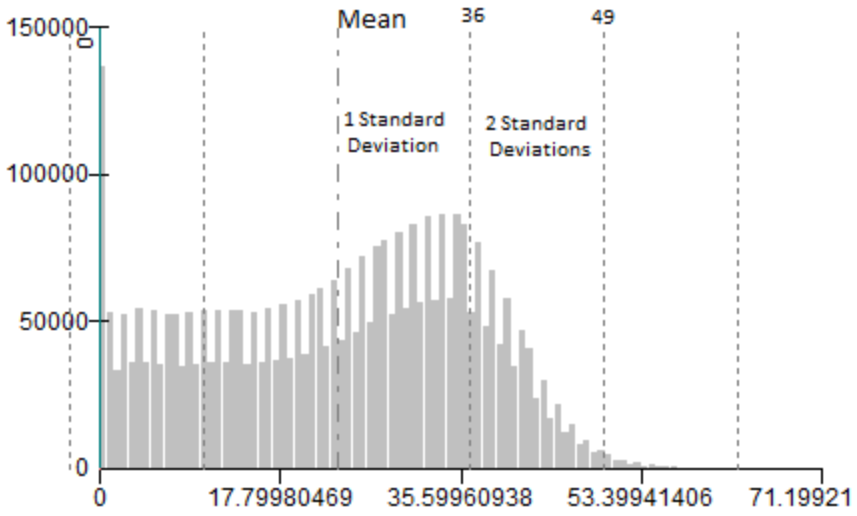

Figure 8b. Histogram for the slopes in the study area

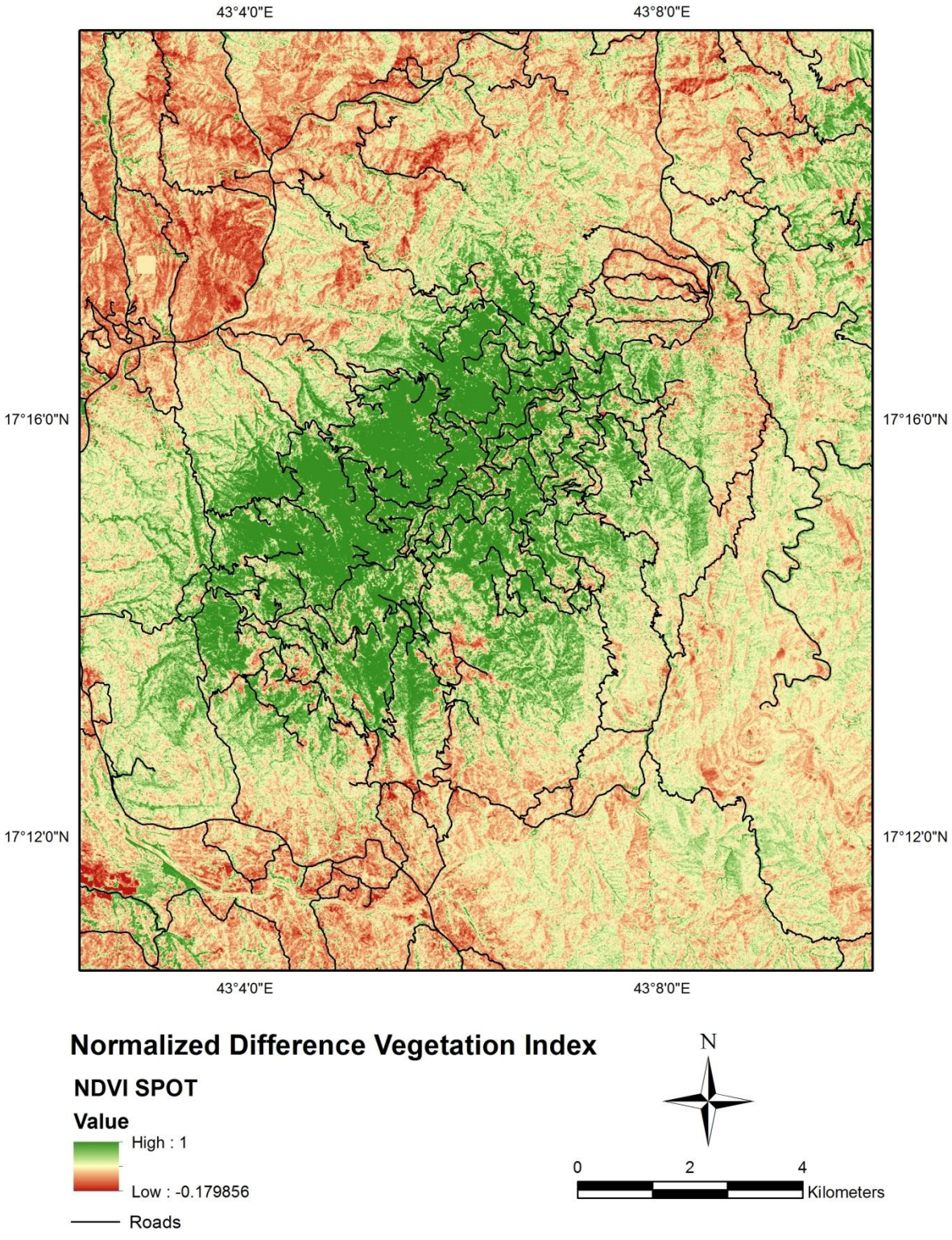

Figure 9a. Color coded NDVI image generated from SPOT image

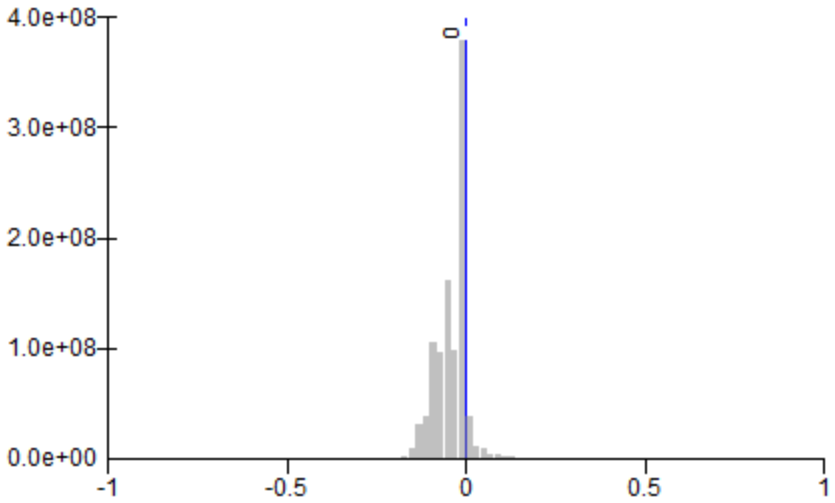

Figure 9b. Histogram for the NDVI in the study area

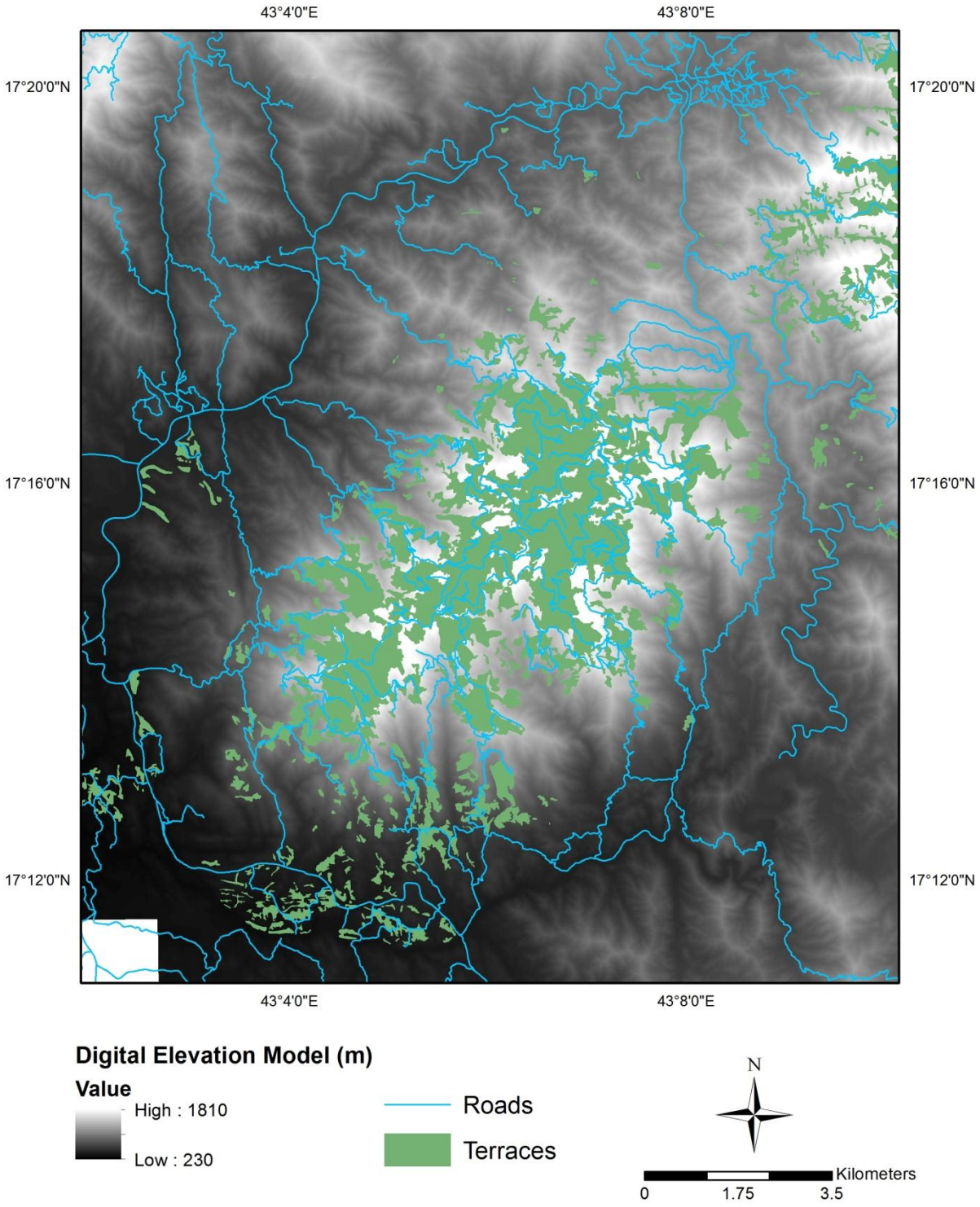

Figure 10. Distribution of terraces extracted from Google Earth images; background digital elevation model.

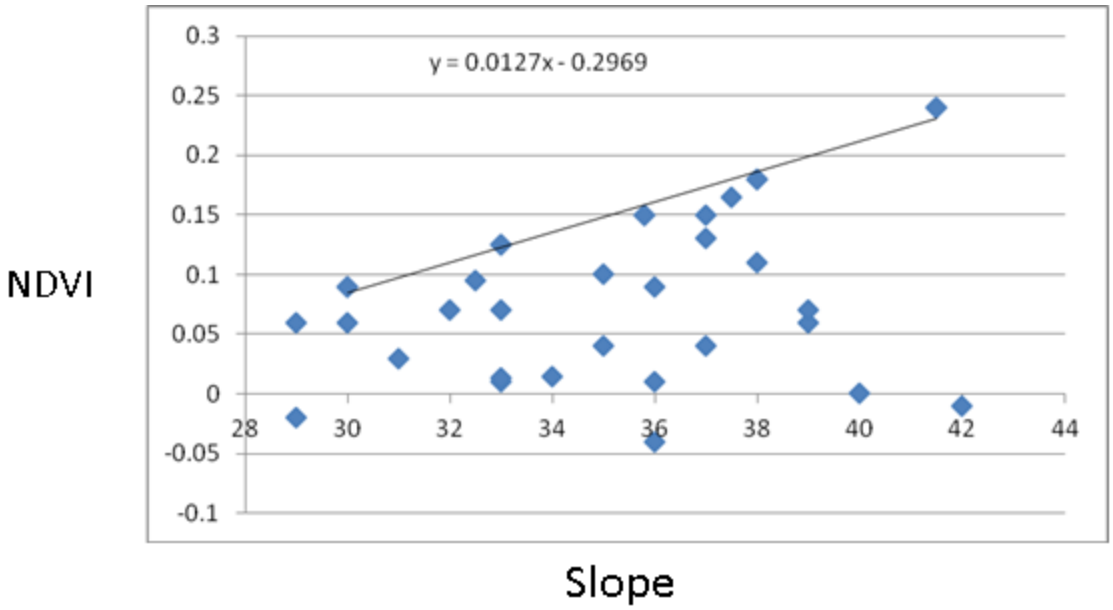

Figure 11. Relationship between NDVI and slope at onset of debris flows

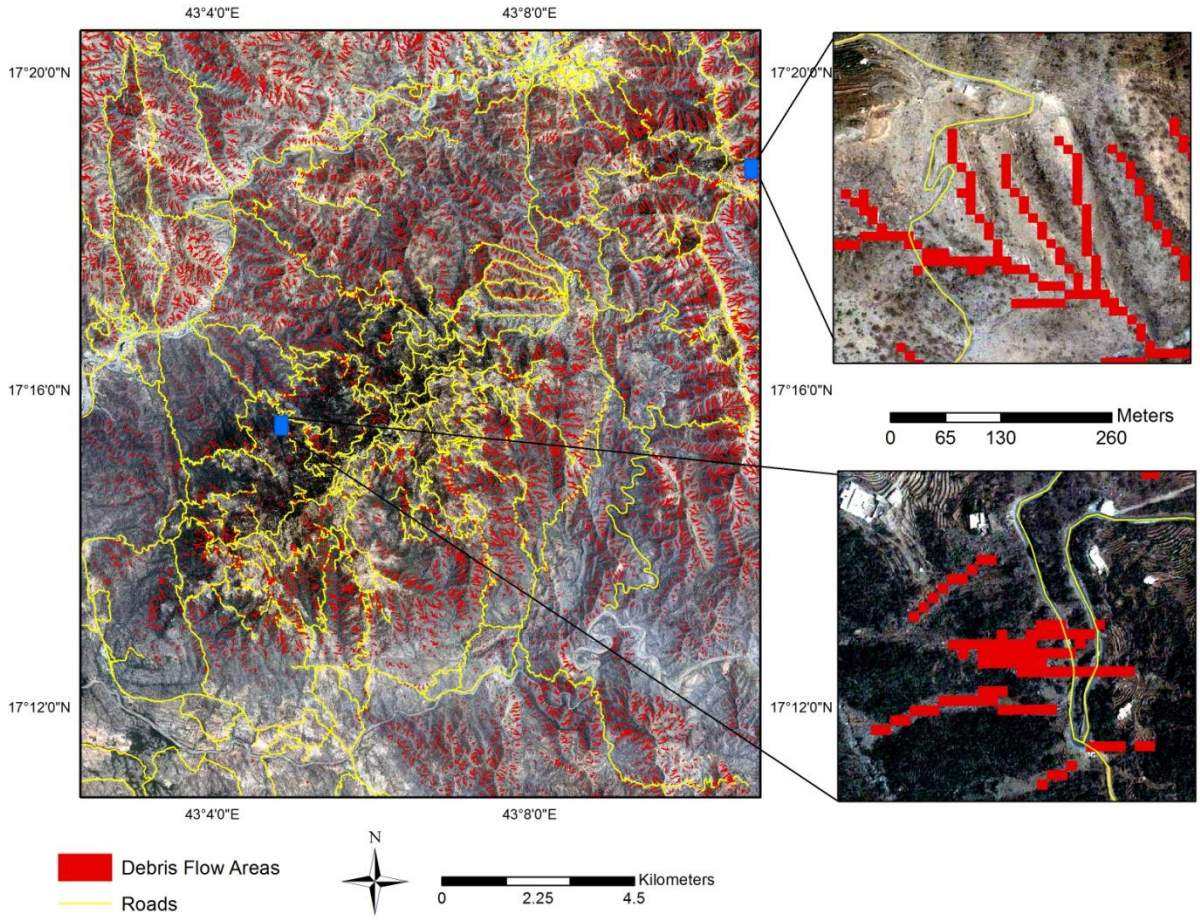

Figure 12. Hazard map showing the distribution of areas prone to debris flows